

Focused laser beams and liquid crystals: fast three-dimensional imaging of structures and topological defects

Ivan I. Smalyukh^{1,*}, Bohdan I. Senyuk², Mingxia Gu², and Oleg D. Lavrentovich^{1,2,#}

¹Liquid Crystal Institute and ²Chemical Physics Interdisciplinary Program,
Kent State University, Kent, OH 44242

ABSTRACT

We show how a tightly focused laser beam can serve as a tool to image complex patterns of the director using the technique of fluorescence confocal polarizing microscopy (FCPM). We expand the capabilities of FCPM into the domain of real-time scanning in order to study the dynamic processes at the time scale of about 1ms. In this approach which we call Fast FCPM, confocal imaging is performed using a modified Nipkow-disc scanning confocal microscope. In the Fast FCPM set up, we use a twisted nematic cell as a fast achromatic polarization rotator to change the polarization of probing light by 90°. The achromatic polarization rotator switches between two orthogonal polarization states when a sufficiently strong electric field is applied to reorient the director structure from the twisted to the homeotropic state. Both FCPM and Fast FCPM employ the property of anisotropic media to align fluorescent dye molecules. When observation is performed in polarized light, the measured fluorescence signal is determined by orientation of the dye molecules. As the dye molecules are aligned by the liquid crystal, the detected fluorescence signal visualizes the spatial patterns of the director rather than concentration gradients of dyes. Finally, we present 3D patterns of director associated with both static and dynamic processes in liquid crystals, anisotropic emulsions, and colloidal suspensions.

Keywords: liquid crystal, fluorescence confocal polarizing microscopy, defect, director structure, colloid

1. INTRODUCTION

Orientalional order is a universal feature of numerous soft-matter systems, most notably liquid crystals (LCs). These systems are extremely flexible, producing a rich variety of complex 3D patterns of orientational order. Molecular interactions responsible for the orientational order are rather weak and director \hat{n} can be easily disturbed by many factors, for example, by magnetic or electric field. It is precisely this sensitivity that explains why LCs are so widely used in modern displays and other electro-optical applications. Non-destructive techniques to study 3D patterns of orientational order are in a great demand. At the same time, fluorescence confocal microscopy (FCM) is broadly used in both materials science and in biology and offers three-dimensional (3D) spatial resolution of about one micron or better¹⁻⁴, but is usually used for the study of 3D positional order in the heterogeneous systems with non-uniform dye distributions¹⁻⁴. In FCM, the inspected region of specimen at a time is a small submicron voxel (=3D pixel). Signals from nearby voxels are suppressed by a special confocal optical design an important element of which is a pinhole in the image space. The pinhole functions as a spatial filter and strongly reduces the signal emerging from outside of the selected voxel. The specimen is usually doped with a high-quantum-yield fluorescent dye that strongly absorbs at the wavelength of the exciting laser beam and fluoresces in spectral range of somewhat longer wavelengths. Two basic features, namely, (a) illumination of a single voxel at a time, and (b) blocking out-of-the-voxel fluorescence signal, improve the resolution of FCM as compared to an ordinary microscope, and, most importantly, allow one to resolve features of the sample along the optical axis of microscope. If the specimen is heterogeneous, the concentration of the fluorescent probe is coordinate-dependent, which results in a high-contrast image. In essence, the FCM technique visualizes the concentration (density) distribution of fluorescence probe in the sample. It is thus well adjusted to study

* Email: smalyukh@lci.kent.edu; Phone 1-330-672-1518

Email: odl@lci.kent.edu; Phone 1-330-672-4844

positionally ordered phases (such as block copolymers) and patterns. The FCM technique makes it possible to visualize features in living cells and tissues; it is successfully applied in flow cytometry and even for single molecule detection. Recently, the improvement of sensitivity of the detectors based on the Charge-Coupled Devices (CCDs) allowed researches to increase the speed of confocal imaging to 1000 frames per second⁵. Usually, fast confocal imaging is based on a Nipkow-disc scanning confocal microscope in which the sample is illuminated by many rather than by one focused beams and the signal is detected through numerous pinholes located in the spinning Nipkow disc⁵.

One of the other recent developments in confocal imaging was adding a feature of polarized light to FCM of liquid crystals and other ordered soft matter systems⁶. This technique, called fluorescence confocal polarizing microscopy (FCPM), allows one to obtain a 3D image of the director field, both in the plane of observation and along the direction of observation⁶. By adding two features, namely, (a) polarized light observations and (b) fluorescent dye composed of anisometric molecules, one transforms the regular FCM into a FCPM that visualizes 3D director patterns, Fig.1a⁶. The technique has been already used to visualize field-induced Frederiks transition in the nematic LCs^{6,7}, focal conic domains in smectic A^{6,8}, disclinations, dislocations^{9,10} and layers undulations¹¹ in cholesteric LCs, director distortions around the particles manipulated by the laser tweezers^{12,13}, director fields in biaxial liquid crystals¹⁴, and director structures and droplet positions in liquid crystal emulsions¹⁵.

In this work we describe the fast 3D imaging of the patterns of molecular orientation using FCPM based on a conventional confocal microscope, Fig.1a, and also Fast FCPM based on the Nipkow-disc scanning confocal microscope. We first describe the experimental approaches and then give examples of 3D imaging of the director fields in a variety of different soft matter systems.

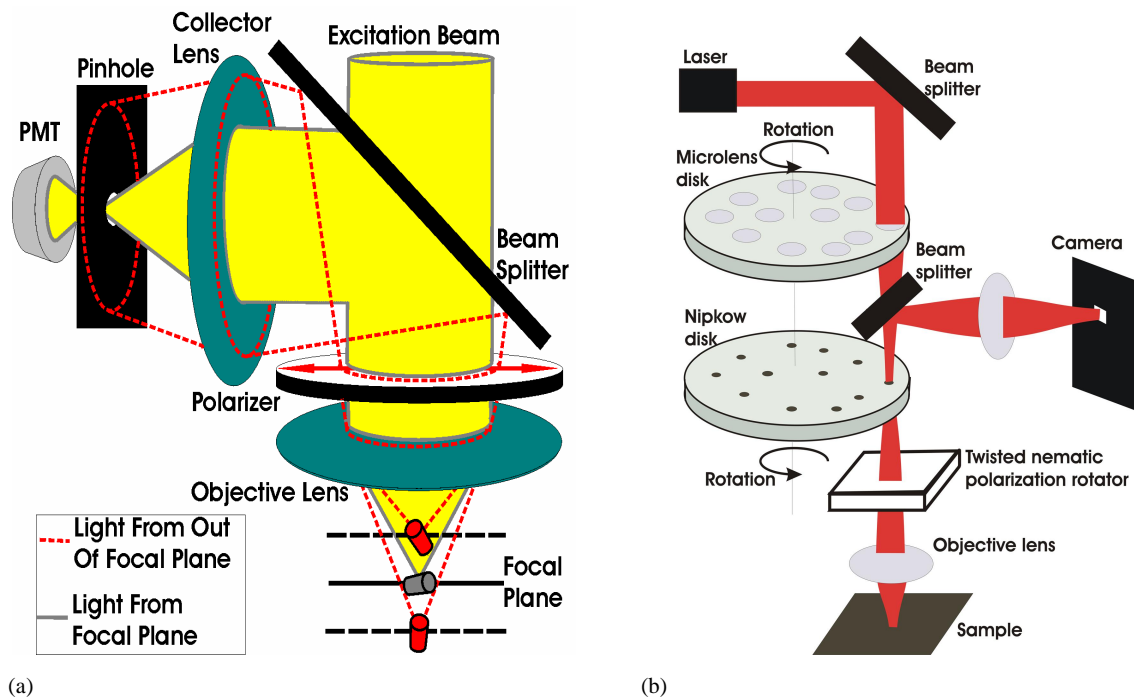


Fig.1. Principal schemes of (a) FCPM based on the Olympus Fluoview BX-50 reflective-mode confocal microscope modified by an addition of a custom rotating polarizer; (b) Fast FCPM based on a Nipkow-disc confocal microscope and a Nikon base; light polarization can be controlled by an electrically switchable twisted nematic cell. Note that only a few pinholes and microlenses are shown in (b).

2. EXPERIMENTAL TECHNIQUES

2.1. Experimental set up of the Fast FCPM

The recent development in the field of fast-scanning microscopy allows one to increase the rate of confocal imaging by three-to-four orders of magnitude, i.e., up to about 1000 frames per second⁵. This fast confocal imaging system is based on the principle of the rotating Nipkow disk with thousands of pinholes, a very old (1884) invention, used in early-stages television. The modern addition⁵ is that the Nipkow disk with pinholes is supplemented by a coaxial disk with micro-lenses. The two discs are mechanically connected and are rotated together by an electrical motor. The micro-lenses focus light onto the pinholes, so that the sample is scanned by thousands of beams at once allowing to increase the speed of imaging by orders of magnitude. The Fast FCPM set up, Fig.1b, is based on the scanning system with a spinning dual Nipkow disk with 20,000 of pinholes and micro-lenses integrated with a Nikon microscope Eclipse E-600 POL base. The microscope is equipped with an accurate (50 nm in setting the vertical position of the focused beam) focus drive. The excitation can be performed in the spectral range between 300 and 900 nm (mercury lamp). The vertical refocusing is performed by a fast piezo z-stepper (PI Piezo) capable of scanning a 10 micron-thick sample by producing 10 frames in less than 5 ms. For repetitive processes, one can use only xy-scanning, refocusing it at different depth step-by step. The speed of imaging depends on many additional factors, such as needed contrast (integration time), size of the scanned area, camera and software, but in majority of situations it can reach 1000 frames per second.

In principle, the polarization direction in FCPM or Fast FCPM can be changed by mechanical rotation of a polarizer which is inserted in the common path for excitation and emission light. However, despite its simplicity, this approach has some disadvantages: 1) the excitation intensity may vary with rotation of a polarizer due to initial partially-polarized state of excitation light in the excitation optical path yet before polarizer; 2) mechanical rotation is slow and allows one to image only stationary director patterns. Another possibility is electro-optical polarization rotator. We equipped the microscope with an achromatic switchable polarization rotator based on a twisted nematic (TN) cell. The achromatic polarization rotator allows one to change the polarization state of probing light within timescale of the order of several milliseconds. We therefore can perform the polarized and non-polarized fluorescence confocal microscopy study of the dynamic changes in orientational order in liquid crystals and other ordered soft matter and biological systems. The confocal system modified by the achromatic polarization rotator preserves its capabilities to visualize the dynamical changes of positional order, such as, for example, motion of beads in colloidal structures (see section 3 of this article).

The design of the polarization rotator based on a twisted nematic cell is such that it combines the advantages of (a) wavelength-independent (within the visible spectral range) switching of the linear polarization, (b) a simple low-voltage (less than 10V AC) driving scheme, and (c) fast switching between the two mutually orthogonal polarization states. The achromatic rotation of linear polarization in the used twisted nematic cell is achieved by satisfying the Mauguin regime condition $M_{\text{au}} = p\Delta n / (2\lambda) = 2d\Delta n / \lambda \ll 1$ (where d is the cell thickness and $p = d/4$ is the pitch of twist, i.e. the distance over which director is twisted for 2π). In the Mauguin regime, the polarization plane is rotated nearly exactly by the angle of twist in the TN cell as light polarization closely follows the director twist. We use a special liquid crystal with very high birefringence ($\Delta n \approx 0.4$) in order to satisfy the above conditions for the relatively thin LC cells ($d = 4\text{-}5$ microns) which allows us for fast switching (about 3-5 milliseconds). The linearly polarized light entering the TN cell is converted into a beam with slightly elliptic polarization at the exit of the polarization rotator, but the ellipticity is small (ratio of light intensities corresponding to the two orthogonal directions is 1:20). The changes of light intensity of the excitation beam caused by switching the polarization rotator are small, less than 5% (as determined by the residual ellipticity of the exit beam and some scattering at director fluctuations of the TN cell). By applying an electric field across the cell, one transforms the twisted nematic state into the polarization-insensitive homeotropic state; this effect allows one to switch the polarization of light between two orthogonal states. According to our experiments, the quality and features of FCPM images taken with the TN polarization rotator were the same as in the mode of observation with a mechanically rotated non-switchable polarizer. The FCPM equipped with the achromatic polarization rotator allows us to electronically switch polarization of the probing light, obtain FCPM textures for different polarization directions within milliseconds, and finally to reconstruct the director structure.

2.2. Basic principles of FCPM imaging

A simple view of how the FCPM visualizes a 3D director field in a nematic sample is as follows. Imagine a nematic LC doped with an anisometric fluorescent dye, such as N,N'-Bis(2,5-di-tert-butylphenyl)-3,3,9,10-perylene-dicarboximide (BTBP)⁶. The transition dipole of the BTBP molecule is oriented along its long axis, Fig.2c. For simplicity, assume that the nematic LC is of a calamitic type (rod-like molecules) and that the fluorescent molecules are also elongated, which is the case of BTBP, Fig.2. The transition dipoles of both excitation and fluorescence are along the long axis of the dye molecule. As it is well known from studies of the so-called "guest-host" display modes, the anisometric "guest" molecules are aligned by the nematic "host". The linearly polarized incident beam (blue wave in Fig.2a-c) causes fluorescence of the dye. The efficiency of light absorption is determined by the angle between the polarization \hat{P} of incident light and the direction of the absorption transition dipole of the dye molecule, usually as $\propto \cos^2 \alpha$, where α is the angle between the dye's transition dipole and \hat{P} , Fig.2c. The excited dye fluoresces (red wave in Fig.2a,c). In the reflective mode FCPM, the fluorescence signal is rooted through the very same polarizer. The intensity of detected light depends on the angle between the polarization direction \hat{P} of the polarizer and the emission transition dipole of the dye, usually as $\propto \cos^2 \alpha$ ^{6,7}. In principle, one can use different schemes of placing the polarizer(s). In our works we usually use a scheme with only one (linear) polarizer that polarizes both the incident and the fluorescent beams, Fig.1. The intensity of detected fluorescence signal is then related to the director orientation as $I \propto \cos^4 \alpha$ ^{6,7}.

It is important to note that the fluorescence lifetime is sufficiently short to assure that the excited dye molecule remains within the given voxel. In liquid crystals, the diffusion coefficient for most dye molecules is of the order of $D \approx 10^{-10} \text{ m}^2 / \text{s}$ ¹⁶. Therefore, to travel the distance of the order of $L = 1 \mu\text{m}$, the dye molecule would need time $t \approx L^2 / D \approx 10 \text{ ms}$, which is much larger than the time during which the fluorescent light is collected in both ordinary FCPM (Fig.1a) and in Fast FCPM (Fig.1b). In other words, the dye molecule will emit within the same voxel in which it was excited. For BTBP dye, the fluorescence lifetime is (3.7-3.9)ns¹⁷, i.e., it is smaller than the characteristic time of rotational diffusion in liquid crystals (~10ns). Therefore, orientations of the transition dipoles of the dye during absorption and emission can be assumed to be close to each other and the intensity of detected fluorescence signal is $I \propto \cos^4 \alpha$ ^{6,7}, as described above. Another important issue is that focusing the laser beam in a birefringent medium is more complicated than in an isotropic medium (since there are two propagating modes with different indices of refraction). To reduce the aberrations one can use a liquid crystal host with a low birefringence Δn : the spatial defocusing of the two modes is $g \Delta n z / \bar{n}$, where \bar{n} is the average refractive index, z is the depth of scanning, and g is a coefficient of the order of unity (dependent on the sample orientation)⁶.

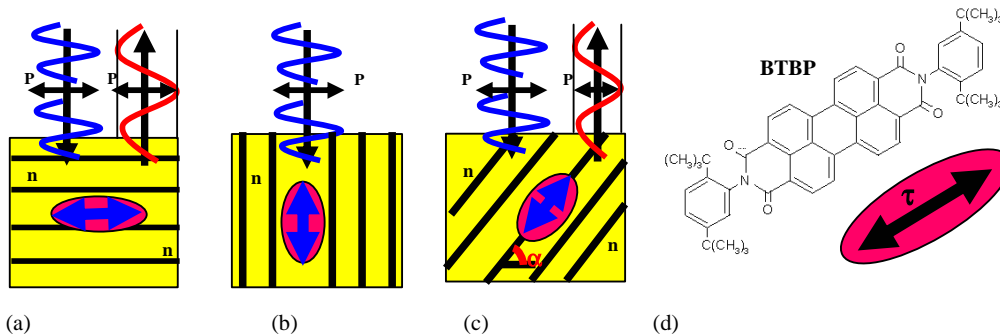


Fig.2. (a-c) Intensity of detected fluorescence of the anisometric dye in a LC host depends on the angle between the transition dipole of the dye molecule and the polarization of light (excitation beam shown as a blue wave, fluorescence beam as a red wave). (d) Anisometric fluorescent dye molecule N,N'-Bis(2,5-di-tert-butyl-phenyl)-3,3,9,10-perylene-dicarboximide (BTBP) solvable in thermotropic LCs with rod-like molecules that aligns with the transition dipole along the LC director.

The FCPM maps the intensity of polarized fluorescent light emitted by the LC sample, rather than the pattern of integrated birefringence as the polarizing microscopy texture does, or the pattern of concentration of fluorescent molecules as the regular FCM does. This feature allows one to avoid the ambiguity of in-plane polarizing microscopy textures that do not distinguish between two mutually perpendicular director configurations^{6, 7}. In the polarizing microscopy observations, the optical phase shift is zero and thus the texture is dark whenever the director is parallel or perpendicular to the polarization of probing light. Because of this, the conventional polarizing microscopy image cannot distinguish between two mutually perpendicular director configurations. FCPM images are free of the $\pi/2$ ambiguity characteristic for the polarizing microscopy observations of the LC textures. If the director (and the transition dipole) is parallel to the polarizer, the intensity of detected light is maximum, Fig.2a. If the director is perpendicular to the polarizer, the intensity is minimum, Fig.2b. More importantly, the confocal scheme of FCPM allows one to collect light from a very small region of the sample at a time and thus to optically slice the specimen by scanning the focused beam allowing for resolving features of orientational order in 3D (including the direction along the optical axis of the microscope). In the following section we provide examples of the non-destructive FCPM imaging of 3D patterns of orientational order in liquid crystals and anisotropic emulsions and suspensions.

3. RESULTS AND DISCUSSION

3.1. Stationary director patterns in nematic liquid crystals and in lyotropic lamellar systems

Figure 3 illustrates how the above principles apply to the director structure of the Frederiks transition in a cell filled with a dye-doped nematic. As the voltage is applied, the originally uniform director \hat{n} , Fig.3a,b, realigns towards the axis Z along the cell normal with the maximum reorientation in the center of the cell, which is manifested by a weaker fluorescence in the corresponding part of the FCPM vertical cross-section, Fig.3c,d. In the case of the example illustrated in Fig.3, the used liquid crystal is a nematic mixture ZLI-3412 and the dye is BTBP.

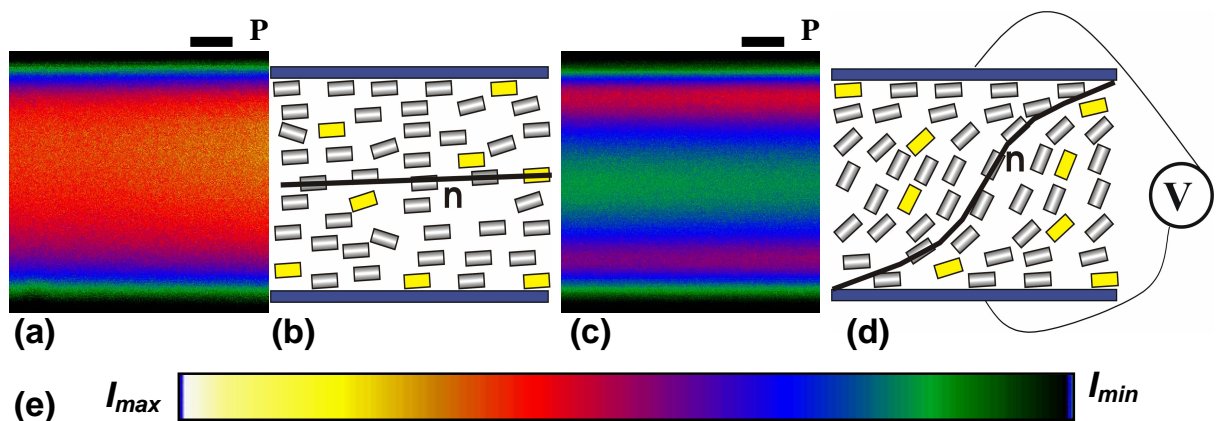


Fig.3. FCPM vertical cross-sections and schematic illustration of director structures associated with the Frederiks transition in a nematic cell: (a,b) uniform \hat{n} , no electric field; (c,d) \hat{n} distorted by the applied voltage; (e) the color-coded intensity scale of the fluorescence signal in FCPM. FCPM textures (a,c) of the vertical cross-section of the cell illustrate the director reorientation observed before and after the transition, respectively.

The studied director distortions in Fig.3 are actually one-dimensional, as the director \hat{n} depends only on Z-coordinate. Figure 4 shows smectic A domains formed in the lyotropic lamellar system, which is a water solution of an amphiphilic material. The samples of the lyotropic ternary system cetylpyridinium chloride (CPCL), hexanol and brine (water +1% NaCl) were prepared according to the following procedures (see Refs.^{18, 19} for more detailed description of preparation of similar lamellar systems). The used fluorescent dyes were first dissolved in hexanol which then was used for the preparation of the lyotropic samples as a co-surfactant. The surfactant CPCL and the dye-doped co-surfactant (hexanol+0.1% of the fluorescent dye) were taken in weight proportion 1:1. The concentration of brine in the studied

samples was within the range 70-80% by weight. The lyotropic lamellar LC was studied in rectangular glass capillaries. The untreated glass of the capillaries sets boundary conditions at the liquid crystal-glass interface for the lamellae of the ternary system to orient parallel to the interface. In most parts of the sample the lamellae are parallel to the confining substrates. The observed deformations in the layers structure are in the form of the so-called focal conic domains (FCDs). The 3D configuration of the director \hat{n} inside the domain is rather complex; the important feature of this structure is that any line that connects a point on the ellipse to a point on the hyperbola, is the local optic axis. FCPM allows one to clearly reconstruct the basic features of this pattern. Figure 4 shows both “horizontal” (parallel to the ellipse, Fig.4a,b) and “vertical” (parallel to the hyperbola, Fig.4d,e) cross-sections of the domains. The FCPM in-plane cross-sections are co-localized with a polarizing microscopy image of the same part of the sample, Fig.4c.

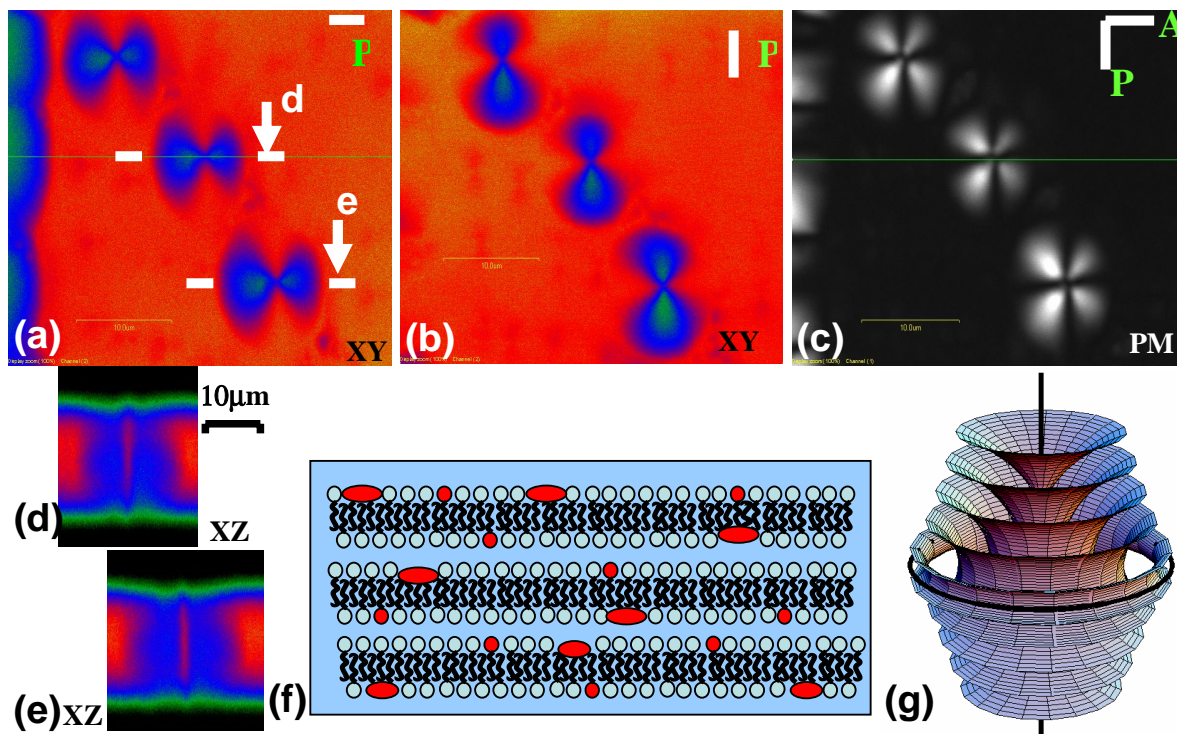


Fig. 4. Focal Conic Domains in the lyotropic L_α -phase of the ternary system cetylpyridinium chloride-hexanol-brine: (a,b) in-plane FCPM cross-sections for different orientations of polarizer P; (c) PM texture of the same part of the LC cell; (d,e) FCPM vertical cross-sections of the focal conic domains marked by “d” and “e” in (a), respectively; (f) schematic illustration of the alignment of the transition dipoles of the DiOC₁₈(3) dye molecules parallel to the lamellae in the lyotropic L_α -phase; (g) layered structure of a focal conic domain different cross-sections of which are visualized by the FCPM in parts (a,b,d,e). The color-coded intensity scale of the fluorescence signal in FCPM is the same as in Fig.3.

We used dye DiOC₁₈(3) in which the transition dipole aligns parallel to the lamellae in the lamellar L_α phase of lyotropic ternary system cetylpyridinium chloride (CPCL), hexanol and brine (water +1% NaCl). The observation that the molecules of DiOC₁₈(3) align with their transition dipoles parallel to lamellae is similar to the prior study for the case of other lyotropic lamellar systems²⁰. As expected for such dye alignment, the fluorescence signal from the parts of cell in which the lamellae are parallel to substrates is much stronger than from the parts of cell in which layers are nearly perpendicular to the cell substrates, Fig.4. In the parts of cell with chains of focal conic domains the fluorescence signal is lower as compared to the homeotropic parts of cell. The appearance of the FCDs changes with rotation of the polarizer (compare parts (a) and (b) in Fig.4) similarly to the case of FCDs in thermotropic smectics,^{6, 8} but now the stronger fluorescence intensity corresponds to unperturbed homeotropic part of the cell rather than to the regions with FCDs. We stress again that this is due to the fact that the DiOC₁₈(3) dye molecules orient parallel to the planes of the

lamellae, Fig.4f, not along the layer normal, director \hat{n} , as in the case of thermotropic smectic⁶. Figure 4g shows a typical layered structure of the focal conic domain that can be reconstructed from the FCPM images, Fig.4a,b,d,e. Note that in Fig.4, the base of FCD is located in the bulk of the lamellar sample; in thermotropic smectic A samples, surface anchoring might cause the bases of FCDs to be located at the boundary⁸.

3.2. Dynamics of defects and director structures.

The examples of the 3D imaging provided above correspond to the static director structures in which the director field is spatially complex but does not change with time, at least on the time scale of hours which is much larger than the time needed to acquire the FCPM images by both types of confocal microscopes shown in Fig.1. The vertical FCPM texture in Fig.5 shows a typical behavior of a vertical $+1/2$ disclination under an external electric field. The surface easy axes are normal to the plane of the image. The disclinations of opposite signs in the applied field become connected by different types of wall defects, Brochard-Leger (BL) wall and the so-called T-wall (a planar soliton stabilized by surface anchoring); the region between the T-wall and the BL-wall is the disclination bending region. The disclination under applied field across the cell experiences translational motion along the wall defects (the motion directionality depends on applied voltage) and also deforms by bending. The polarization of the probing light has been chosen along the normal to the FCPM image in order to increase the contrast between the T-wall and the BL-wall. The strong fluorescence intensity from the BL-wall shows that the director \hat{n} in this region is oriented along the polarization direction in the FCPM (normal to the vertical cross-section). In the region corresponding to the T-wall the fluorescence signal is much weaker, illustrating that \hat{n} is oriented in the plane of the image (perpendicular to the polarization), Fig.5. The T-wall and the BL-wall are clearly seen as separated by a bent disclination line, Fig.5. The above example illustrates the capability of FCPM to visualize the 3D director structures changing with time; for detailed study of the disclination bending dynamics we refer the reader to Ref.²¹.

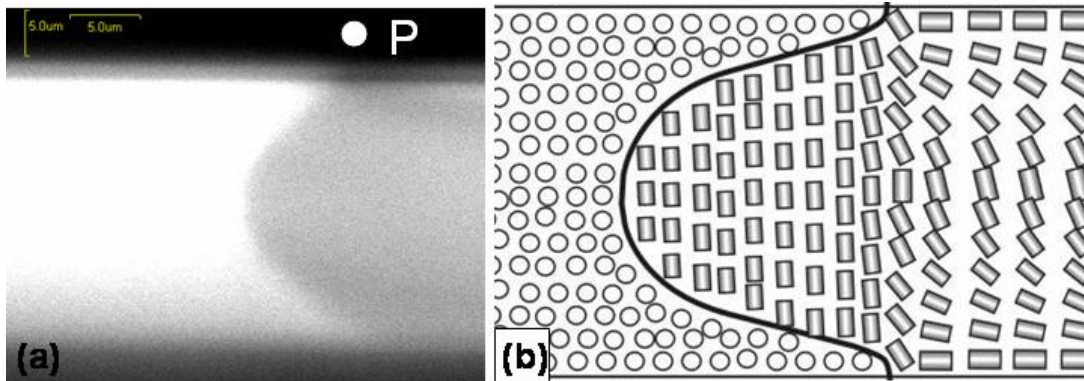


Fig.5. FCPM cross-section and the director field characterizing a $+1/2$ disclination bending behavior under electric field. (a) vertical FCPM cross-section in the plane containing the T-wall (to the left from the disclination) and the BL-wall (to the right from the disclination); (b) the reconstructed director structure with the disclination marked by a thick black line.

3.3. FCPM imaging of stationary structures and dynamic processes in anisotropic colloidal systems.

Now we will discuss the FCPM imaging of heterogeneous systems such as liquid crystal emulsions and suspensions. As we shall see, FCPM allows one to decipher not only spatial positions of colloidal inclusions in the liquid crystal matrix, but also the director structures in the liquid crystal associated with these inclusions. Recently, we used confocal microscopy to demonstrate that placement of colloidal particles (glycerol droplets of radius $R=1-10$ microns) at the LC surface leads to attractive interactions and a variety of ordered patterns, including the hexagonal patterns and chains¹⁵. Below we use a similar liquid crystal colloidal emulsion to illustrate FCPM imaging of both positional and orientational order in the anisotropic emulsions, Fig.6. The glycerol droplets are obtained as in Ref.¹⁵. A Petri dish containing a layer of glycerol and the nematic LC pentylcyanobiphenyl (5CB, EM Industries) on top of it, is kept at about 50°C for 10 min, to facilitate diffusion of the glycerol molecules into the 5CB layer which is in the

isotropic phase above $\sim 35^{\circ}\text{C}$. When the sample is cooled down, solubility of glycerol in 5CB decreases and one observes appearance and growth of glycerol droplets. The technique produces droplets of a practically constant radius in the films of controlled thickness which is in the range $h=(1-100)$ microns. The size of droplets is controlled by the cooling rate and thermal cycling. The 5CB film is in the so-called hybrid aligned state, as the director \hat{n} is parallel to the LC-glycerol interface at the bottom and perpendicular to the air-LC interface at the top.

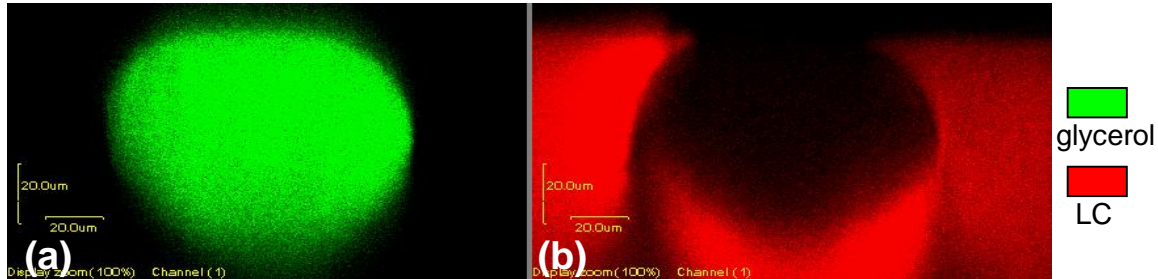


Fig.6. FCPM vertical cross-section of a glycerol droplet at the liquid crystal-air interface: (a) fluorescence from glycerol doped with fluorescein; (b) polarized fluorescence signal from the liquid crystal doped with the Nile Red dye.

Two different dyes with well separated absorption and fluorescence bands, fluorescein and Nile red (both purchased from Aldrich), were added in small quantities (0.01 wt %) to tag glycerol and LC, respectively. The molecules of fluorescein are relatively polar and their solubility in glycerol is much better than in LC. Therefore, after the phase separation of glycerol and LC, the Fluorescein molecules stay in glycerol, which are also polar and contain similar hydroxyl groups as the dye molecules. The molecules of Nile Red have hydrophobic tails and anisometric shape, similarly to the used liquid crystals (5CB, E7, ZLI-3412, ZLI-2806). Nile Red has much better solubility in the LC and, therefore, after the phase separation of glycerol and LC it stays in the liquid crystal. The Nile red molecules are well oriented by the LC host, which allows one to determine the 3D director patterns¹⁵. Addition of the dyes did not change the appearance of patterns of droplets and director structures¹⁵. The maximum absorption wavelength of Fluorescein coincides with the wavelength of excitation by Ar Laser, 488nm, whereas the Nile Red dye is efficiently excited by Kr Laser at wavelength 568nm. The emission crosstalk between the two fluorophores is sufficiently small and allows one to separate the fluorescent signals from the two different dyes using interference filters. The fluorescent signal from Fluorescein dye is detected in the wavelength region 510-550nm, whereas the fluorescent signal from Nile Red is detected in the spectral range 585-650nm.

The FCPM textures of vertical cross-section of the samples, Fig.6, unambiguously demonstrate that the glycerol droplets are trapped at the LC-air interface; clearly, the top of the glycerol droplets is protruding from the nematic film. The polarized fluorescence signal from liquid crystal layer visualizes director distortions in LC around the droplet¹⁵. For a better clarity, the images in Fig.6 are taken for a relatively large droplet and a thick liquid crystal layer; smaller drops are also located at the interface and they produce similar director distortions¹⁵. Detailed study of the colloidal structures and director distortions in the similar liquid crystal emulsions is described in Ref.¹⁵.

The above example of FCPM imaging in a liquid crystal emulsion corresponds to a stationary structure in a heterogeneous system. Another degree of complexity to the FCPM imaging is added if one studies dynamic processes in the anisotropic emulsions or suspensions. A simple example of such a dynamic process in anisotropic emulsion is Brownian motion of a colloidal particle in the bulk of a liquid crystal medium, Fig.7a. A polymer micro-particle with tangential boundary conditions (made of melamine resin and additionally treated with polyisoprene for tangentially degenerate anchoring) produces director distortions of quadrupolar symmetry when introduced into a liquid crystal matrix with the uniform far-field director \hat{a} , Fig.7a. Using FCPM, we determine the director configurations in the cell (by detecting fluorescence of BTBP detected in the spectral range 510-550nm) as well as the positions of the polymer particles (by detecting fluorescence from Rhodamine B embedded into the spheres, detection spectral range 575-650nm). Using fluorescence from the dye-labeled particle and a special fitting procedure, one can determine the particle location in the liquid crystal medium; this can be done rather precisely, with spatial resolution in the range 5-10nm. Fig.

7b shows spatial displacements from their original positions (taken to be at the origin of the coordinate system) of the bead during constant periods of time (15 milliseconds); the corresponding histograms for each coordinate are shown in Fig.7c,d. As the particle undergoes Brownian motion, the director distortions around it on average retain quadrupolar symmetry, Fig.7a.

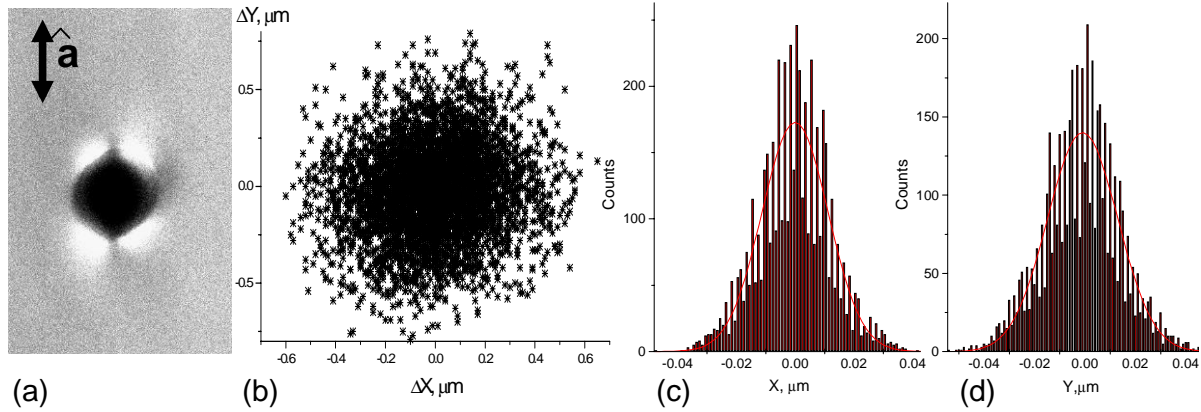


Fig.7. (a) In-plane FCPM texture of director distortions around a spherical particle of $3\mu\text{m}$ diameter with tangential anchoring; (b) the displacement of the particles undergoing Brownian motion in the plane of the cell, (c,d) the corresponding histograms for each coordinate. The far-field uniform director in (a) is marked by a double arrow and “ \hat{a} ”. To obtain the data for part (b) the position of the particle was recorded every 15 ms.

When the number of particles in the liquid crystal suspension is sufficiently large so that the inter-particle distances are of the order of several particle diameters, the beads start to aggregate into chains as a result of elasticity-mediated colloidal interactions²². Unlike in the case of particles with homeotropic anchoring which usually form chains along the far-field director^{23,24}, the beads with tangential anchoring aggregate into chains directed at about 30 degrees from the far-field director, Fig.8a,b.

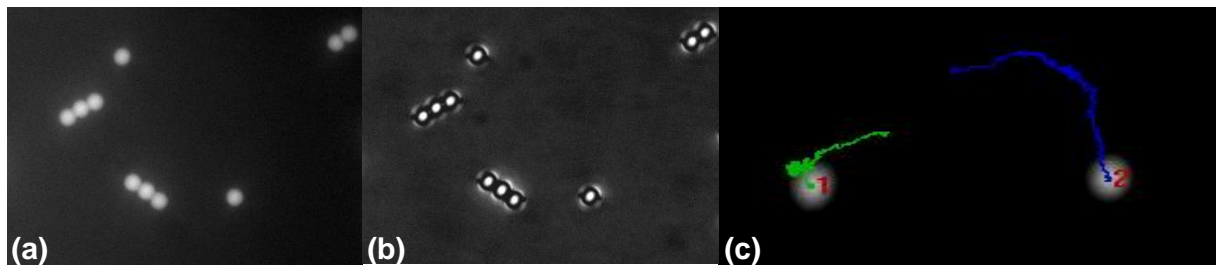


Fig.8. FCPM imaging of spatial positions of the spherical particles, director distortions associated with these solid spheres, their colloidal interactions, and aggregation in the bulk of a nematic LC: (a) in-plane FCPM image of the fluorescently labeled beads aggregating in the nematic host; (b) in-plane FCPM texture of director distortions produced by the particles with tangential anchoring (aggregating into chains) co-localized with the fluorescence signal from the particles; (c) trajectories of particle motion when they are released with the initial separation along the far-field director \hat{a} . The formation of chains of particles is visualized using fluorescence from BTBP (showing distortions of the director, channel #1, part b) and using fluorescence from Rhodamine B embedded in the polymer spheres (showing spatial location of the particles, channel #2, part a). The far-field director and the polarization direction in FCPM are both along the long sides of the photographs (a-c). Part (c) shows the initial positions of the particles and trajectories of their motion as they interact with each other in the uniformly aligned nematic host.

To characterize the pair interaction, we used a dual beam laser trap²². Two particles are trapped at different locations and then released by switching off the laser²². Their motion is strongly influenced by Brownian motion when

the inter-particle-separation is larger than 3-4 particle diameters, but the anisotropic colloidal interactions become noticeable at smaller separations. The attracting particles eventually touch at about 30 degrees with respect to the far-field uniform director \hat{a} . Figure 8c illustrates the trajectories of particle motion in the liquid crystal matrix as they attract each other. For the detailed study of colloidal interactions and aggregation of particles with tangential anchoring we refer the reader to Ref. ²²

4. CONCLUSION

The examples above illustrate that the Fluorescence Confocal Polarizing Microscopy can be successfully used for many problems in different soft matter systems, whenever one is interested in orientational features of molecular organization. Using special dyes and polarized light, one can get an access not only to the spatial positional 3D pattern, but also to the 3D pattern of molecular orientation. We showed that FCPM can be used not only in the studies of relatively simple and spatially homogeneous samples (in terms of composition), but also in the studies of heterogeneous systems, such as nematic emulsions and colloidal suspensions. We also demonstrated that FCPM is capable of imaging not only stationary patterns of molecular orientation, but also the director structures that change in time and are associated with motion of particles, defects, colloidal interactions, etc. Finally, orientational order is featured not only by the classical thermotropic liquid crystals, but also by other soft-matter systems and biologically relevant materials. Both FCPM and Fast FCPM techniques are applicable to the studies of these systems, as we demonstrated by an example with a FCPM imaging of structural distortions in a water-based lyotropic lamellar phase.

5. ACKNOWLEDGMENTS

We thank L. Longa, Yu. Nastishin, M. Kleman, V. Pergamenschik, and S. Shiyonovskii for discussions. We acknowledge partial support of the NSF Grant DMR-0315523. Ivan I. Smalyukh acknowledges the Postdoctoral Fellowship of the Institute of Complex and Adaptive Matter.

REFERENCES

1. T. Wilson, *Confocal Microscopy*, Academic Press, London, 1990.
2. T. R. Corle and G. S. Kino, *Confocal Scanning Optical Microscopy and Related Imaging Systems*, Academic Press, San Diego, CA, 1996.
3. C. J. R. Sheppard and D. M. Shotton, *Confocal Laser Scanning Microscopy*, BIOS Scientific Publishers, Oxford, 1997.
4. R. H. Webb, *Confocal Optical Microscopy*, *Rep. Prog. Phys.* **59**, 427-471 (1996).
5. T. Tanaami, S. Otsuki, N. Tomosada, Y. Kosugi, M. Shimizu, and H. Ishida, "High-Speed 1-frame/ms scanning confocal microscope with a microlens and Nipkow disks," *Applied Optics* **41**, 4704-4708 (2002).
6. I. I. Smalyukh, S. V. Shiyonovskii, and O. D. Lavrentovich, "Three-Dimensional Imaging of Orientational Order by Fluorescence Confocal Polarizing Microscopy," *Chem. Phys. Lett.* **336**, 88-96 (2001).
7. S. V. Shiyonovskii, I. I. Smalyukh, and O. D. Lavrentovich, "Computer simulations and fluorescence confocal polarizing microscopy of structures in cholesteric liquid crystals," In: *Defects in Liquid Crystals: Computer simulations, theory and experiment*, Editors: O. D. Lavrentovich, P. Pasini, C. Zannoni, and S. Zumer, Vol. 43, pp.229-270, Kluwer Academic Publishers, the Netherlands, 2001.
8. O. P. Pishnyak, Yu. A. Nastishin, and O. D. Lavrentovich, Comment on "Self-organized periodic photonic structures in a non-chiral liquid crystal", *Phys. Rev. Lett.* **93**, 109401 (2004); I. I. Smalyukh, D. J. Termine, S. V. Shiyonovskii, and O. D. Lavrentovich, "Three-Dimensional Imaging of Liquid Crystals", *G.I.T. Imaging and Microscopy* **3**, 16-19 (2001); also published in *G.I.T. Laboratory Journal, Europe* **6**, 118-120 (2002).

9. I. I. Smalyukh and O. D. Lavrentovich, "Three-dimensional director structures of defects in Grandjean-Cano wedges of Cholesteric liquid crystals studied by fluorescence confocal polarizing microscopy," *Phys. Rev. E* **66**, 051703/1-16 (2002).
10. I. I. Smalyukh and O. D. Lavrentovich, "Anchoring-mediated interaction of edge dislocations with bounding surfaces in confined cholesteric liquid crystals," *Phys. Rev. Lett.* **90**, 085503/1-4 (2003).
11. B. I. Senyuk, I. I. Smalyukh, O. D. Lavrentovich, "Switchable two-dimensional gratings based on field-induced layers undulations in cholesteric liquid crystals," *Opt. Lett.* **30**, 349-351 (2005).
12. I. I. Smalyukh, A. N. Kuzmin, A. A. Kachynskii, P. N. Prasad, and O. D. Lavrentovich, "Optical trapping of colloidal particles and measurement of the defect line tension and colloidal interaction forces in a thermotropic nematic liquid crystal," *Appl. Phys. Lett.* **86**, 021913/1-3 (2005).
13. I. I. Smalyukh, B. I. Senyuk, A. N. Kuzmin, A. V. Kachynski, P. N. Prasad, S. V. Shiyonovskii and O. D. Lavrentovich, "Optical trapping, manipulation, and 3D imaging of disclinations in liquid crystals and measurement of their line tension," *Mol. Cryst. Liq. Cryst.*, accepted (2005).
14. I.I. Smalyukh, R. Pratibha, N.V. Madhusudana, and O.D. Lavrentovich, "Selective Imaging of 3D Director Fields in Biaxial Lamellar Liquid Crystals," *European Phys. J. E* **16**, 179-191 (2005).
15. I. I. Smalyukh, S. Chernyshuk, B. I. Lev, A. Nych, U. Ognysta, V. G. Nazarenko, and O. D. Lavrentovich, "Ordered droplet structures at the liquid crystal surfaces and elastic-capillary colloidal interactions," *Phys. Rev. Lett.* **93**, 117801/1-4 (2004).
16. L. M. Blinov and V. G. Chigrinov, *Electrooptic Effects in Liquid Crystal Materials*, Springer, New York, 1994.
17. W. E. Ford, P. V. Kamat, "Photochemistry of 3,4,9,10-perylene-tetracarboxylic dianhydride dyes. 3. Singlet and triplet excited-state properties of the bis(2,5-di-tert-butylphenyl)imide derivative," *J. Phys. Chem.* **91**, 6373-6380 (1987).
18. P. Boltenhagen, O. D. Lavrentovich, and M. Kleman, "Oily streaks and focal conic domains in L_α lyotropic liquid crystals," *J. Phys. II France* **1**, 1233-1252 (1991).
19. Yu. A. Nastishin, "Brine-rich corner of the phase diagram of the ternary system cetylpyridinium chloride-exanol-brine," *Langmuir* **12**, 5011-5015 (1996).
20. J.Yguerabide and L. Stryer, "Fluorescence spectroscopy of an oriented model membrane," *Proc. Nat. Acad. Sci. USA*, **68**, 1217-1221 (1971).
21. A. Vella, R. Intartaglia, C. Blank, I. I. Smalyukh, O. D. Lavrentovich, and M. Nobili, "Electric Field Induced Deformation Dynamics of a Single Nematic Disclination," *Phys. Rev. E*, **71**, 061705/1-10 (2005).
22. I. I. Smalyukh, O. D. Lavrentovich, A. N. Kuzmin, A. V. Kachynski, P. N. Prasad, "Elasticity-mediated self-organization and colloidal interactions of solid spheres with tangential anchoring in a nematic liquid crystal", submitted (2005).
23. P. Poulin, H. Stark, T. Lubensky, and D. Weitz, "Novel colloidal interactions in anisotropic fluids," *Science* **275**, 1770-1773 (1997).
24. J.-C. Loudet, P. Barois, and P. Poulin, "Colloidal ordering from phase separation in a liquid-crystalline continuous phase," *Nature* **407**, 611-613 (2000).